Desalination and Water Treatment
www.deswater.com
doi: 10.5004/dwt.2018.22778

123 (2018) 277–287
August

Adsorptive removal of Cr^{3+}, Cu^{2+}, and Ni^{2+} ions by magnetic Fe_3O_4@alkali-treated coal fly ash

Ya-Na Zhang[a,b], Yang-Xin Yu[a,*]

[a]*Laboratory of Chemical Engineering Thermodynamics, Department of Chemical Engineering, Tsinghua University, Beijing 100084, China, Tel. +8610-62782558; Fax: +8610-62770304; email: yangxyu@mail.tsinghua.edu.cn (Y.-X. Yu)*
[b]*State Key Laboratory of Organic–Inorganic Composites, Beijing University of Chemical Technology, Beijing 100029, China*

Received 27 February 2018; Accepted 1 July 2018

ABSTRACT

With the rapid development of industrial economy, water pollution by heavy metals is becoming more and more serious and efficient treatment of the polluted water is still a challenge. To solve this problem, we synthesized magnetic nanoparticles of Fe_3O_4@alkali-treated coal fly ash (MNFFA) by the coprecipitation method at 298.15 K and 101.3 kPa. The structures of the MNFFA were characterized by the scanning electron microscope, X-ray diffraction, and surface area analyses. The effects of adsorbent composition and dosage, equilibration time, temperature, pH, and co-existing ions on the adsorption were investigated to optimize the operating condition for the removal of Cr^{3+}, Cu^{2+}, and Ni^{2+} ions by the MNFFA. The adsorption equilibrium and kinetics follow the Langmuir isotherm and pseudo-second-order kinetic model, respectively. The adsorption capacity was calculated to be 212.3, 229.9, and 26.2 mg/g for Cr^{3+}, Cu^{2+}, and Ni^{2+}, respectively, by fitting equilibrium data to the Langmuir model. The selectivity of Cu^{2+} over Cr^{3+} and Ni^{2+} is, respectively, 1.06 and 8.68 in the binary cationic solutions and 1.21 and 4.67 in the ternary cationic solution. The high adsorption capacity was kept after five cycles, indicating that the adsorbent is stable enough to be regenerated and re-used efficiently. The results demonstrated that the MNFFA is an effective, low-cost, and environment-friendly adsorbent and therefore is very promising to be applied in the adsorptive removal of the heavy metal ions from polluted water.

Keywords: Magnetic nanoparticles, Fe_3O_4@alkali-treated coal fly ash; Adsorption; Heavy metal ion; Kinetics; Water treatment

1. Introduction

In the process of industrialization and urbanization, massive and uncontrolled discharge of heavy metal ions into aquatic streams has seriously polluted the biotic resources [1]. Heavy metals in the environment can originate from both natural and anthropogenic sources and the pollution has become one of the most serious environmental problems not only in China but also around the world. Large numbers of people are threatened by heavy metal pollution. Extensive damage to human organs, such as liver, kidney, digestion system, and nervous system can be caused by uptake of excess heavy metals [2–4]. Although severe contamination of heavy metals has been known to be a major environmental problem for decades, it is getting worse in recent years and there are few feasible approaches to solve this problem. Removal of heavy metal ions from water or various industrial effluents before they discharge indiscriminately is still a great challenge for the scientists in the field of chemical and environmental engineering and management.

The removal of heavy metal ions from aqueous solutions has been commonly carried out by several processes including chemical precipitation, solvent extraction, ion-exchange, electrode-deposition, membrane filtration, flotation, oxidation–reduction, reverse osmosis, biosorption, and adsorption [2,5–7]. All these methods except adsorption have weaknesses such as energy-extensive consumption, high cost,

* Corresponding author.

1944-3994/1944-3986 © 2018 Desalination Publications. All rights reserved.

generation of secondary pollutants, complicated process, or poor removal efficiency. Adsorption processes are worldwide adopted in the field of environmental protection, thanks to the ability of certain solids to preferentially concentrate specific substances onto their surface, such as heavy metals and organics. The adsorption proves to be a simplest and most cost-effective technique and a wide range of adsorbents have been developed and tested for the fast removal of metal pollutants from wastewaters [8]. Nevertheless, better adsorbents are expected to be developed to improve the adsorption efficiency for heavy metal ions.

It is attractive to use natural materials and industrial wastes as an alternative to chemically synthesize adsorbents. Coal fly ash is an industrial waste with characteristics of excellent adsorbents, such as relatively large surface areas, well-defined pore sizes, high pore volume and high adsorption capacity, ease of modification, and diversity composition [9–11]. As a low-cost adsorbent, coal fly ash has been used for the management of heavy metals very early. Researchers have tried different modification methods for improving the adsorption performance of fly ash. These include acid-, alkali-, salt-, surfactant-, mix- and hydrothermally modifications as well as synthesize zeolites [11–20]. The adsorption capacity is greatly dependent on the modification methods used. For instance, Hui et al. [14] used zeolite 4A to remove Cr^{3+}, Cu^{2+}, and Ni^{2+} from the wastewater. The adsorption capacity of the three kinds of ions is 32.52, 23.58, and 3.87 mg/g at pH = 3.0, and 56.47, 72.73, and 4.95 mg/g at pH = 4.0, respectively. In contrast, Kelleher et al. [15] reported that the adsorption capacity of Cr^{3+} is 52.6–106.4 mg/g at 20°C–40°C by using fly ash or modified fly ash.

Extensive investigations [21–26] exposed that the above methods have a common weak point in the separation of solid–liquid phases after adsorption. A good way to overcome this weakness is to separate the solid–liquid phases using magnetic technology [27]. Magnetic nanoparticles of Fe_3O_4 or $NiFeO_4$ can be modified by covalent binding or coatings with van der Waals interactions to inhibit the aggregation. Trisodium citrate [28,29], 3-[2-(2-aminoethylamino) ethylamino] propyltrimethoxysilane [30], N-doped mesoporous carbon [31], metal-organic frameworks [32], *g*-C_3N_4/$FeVO_4$ [33], BiOCl/*g*-C_3N_4/Cu_2O [34], coal fly ash [35], and other substances have been utilized for this purpose. The greatest advantage of this process is that an easy, faster, simpler separation of the metal ions loaded on the magnetic adsorbent from solution can be achieved using an external magnetic field compared with those used traditionally. In addition, desired materials are separated from solution without any secondary wastes. Coal fly ash is of great yield and needs to be effectively disposed of. However, there are few research on the synthesis of magnetic nanoparticles of Fe_3O_4-fly ash (MNFFAs) [35]. Only Chen et al. [35] synthesized Fe_3O_4-fly ash composites by liquid phase deposition method, where the coal fly ash was used without any pretreatment. Currently, there is no report about removal of Cr^{3+}, Cu^{2+}, and Ni^{2+} ions by using MNFFAs in literature [16]. Thus, an efficient, economic, scalable, and nontoxic synthesis of MNFFAs is highly desired for the removal of these heavy metal ions.

Herein, the MNFFAs were synthesized by coating Fe_3O_4 with NaOH-activated coal fly ash, which is slightly different from that reported by Chen et al [35]. The kinetics and thermodynamics for the sorption of Cr^{3+}, Cu^{2+}, and Ni^{2+} on the prepared samples were investigated. The effects of several operating parameters on the adsorption capacity and selectivity were experimentally obtained.

2. Materials and methods

2.1. Materials

The coal fly ash sample was obtained from Zhengzhou Second Power Plant, Henan, China. The fly ash particle size is in the range of 0.5–300 μm. It is composed of 58% (wt%) of SiO_2, 30% of Al_2O_3, 4.3% of FeO, 1.5% of CaO, 2.8% of MgO, and 3.4% of Na_2O. All other reagents with analytical grade were purchased from Beijing Chemical Reagents Company and used as received.

2.2. Preparation of MNFFA

Under a certain speed of stirring, the coal fly ash (50 g) was treated for 30 min in 100 mL NaOH (1.0 mol/L) solution. Then, the solid–liquid mixtures were filtered, cleaned several times with the distilled water, and then dried the alkali-treated fly ash using a vacuum drying oven at 333.15 K for at least 12 h. In order to obtain a sufficient quantity of alkali-modified samples for the subsequent preparation, the preceding steps were repeated several times.

A certain quantity of 0.1 mol/L $FeCl_3$, 0.1 mol/L $FeSO_4$, and 1.0 mol/L NaOH solutions was added into a beaker (250.0 mL) and stirred with a certain speed for 30 min. Then the alkali-modified fly ash filtered above was introduced to the reaction solution and reacted for 2 h. The mass ratio of the alkali-modified fly ash and the $FeCl_3$-$FeSO_4$-NaOH solution, hereinafter referred to as solid/liquid (*S*/*L*) ratio, were studied at *S*/*L* = 1/5, 1/10, 1/15, 1/20, and 1/25. After adsorption the solid–liquid mixture was separated by applying a magnetic field. The product of the MNFFA was washed by the deionized water and then dried in the oven at 333.15 K for 12 h.

2.3. Characterization of MNFFA

Our study focuses on the adsorption capacity of metal ion on the prepared adsorbents and scanning electron micrographs (SEM), X-ray diffraction (XRD), and Brunauer–Emmett–Teller (BET) method can catch the main characteristics of prepared adsorbents although the Fourier transform infrared spectroscopy, vibrating sample magnetometer, SEM with energy dispersive X-ray spectroscopy, etc. could be used to characterize the samples before and after adsorption for detailed structural properties. The MNFFAs were characterized using the SEM (TM3000, Hitachi, Japan) and specimens were coated with gold for 30 s in SEM-coating equipment. Their crystal phases were analyzed using the BTX-Profiler XRD (America). The specific surface area of the sample was calculated by the BET method, and the pore volume was evaluated from the desorption branch of the isotherm based on the Barrett–Joyner–Halenda (BJH) model. During the adsorption procedure, all batch experiments were carried out by adding 100 mL solution with an ionic concentration of 100 mg/L and a certain quantity of dry adsorbent into a 250 mL beaker.

2.4. Analytical methods

The concentration of heavy metal ions was determined by an atomic absorption spectrometer. The calibration curve was obtained by preparing standard solutions with concentrations of same interval ranging from 0 to 25 mg/L. The final data were the average values of at least three experiments, and the standard deviations were less than 2.0%.

The equilibrium adsorption capacity, q_e (mg/g), and removal efficiency, η_e (%), were calculated according to the following equations:

$$q_e = \frac{(C_0 - C_e)V}{W} \quad (1)$$

$$\eta_e = \frac{(C_0 - C_e)}{C_0} \times 100 \quad (2)$$

where C_0 and C_e are the initial and equilibrium heavy metal ions concentrations (mg/L), respectively. V is the volume of solution (L) and W is the weight of adsorbent (g) used in the adsorption experiments.

3. Results and discussion

3.1. Characteristics of adsorbents

Figs. 1(a)–(d) show the SEM images of the original and MNFFA in different magnifications. Figs. 1(a) and (b) and Figs. 1(c) and (d) are with the magnification of 2,000 and 9,000 times, respectively. As can be seen from Figs. 1(a) and (b), the surface of the original fly ash is relatively smooth, and the MNFFA is rougher. It could be concluded that the surface area of the MNFFA with S/L = 1:20 ($MNFFA_{1:20}$) is larger than that of the original fly ash. Besides, the $MNFFA_{1:20}$ has more channels than pure fly ash as can be inferred from the comparison between Figs. 1(d) and (c). Thus, the $MNFFA_{1:20}$ is expected to have a higher adsorption activity.

The pore size distribution dV_p/dD_v of the $MNFFA_{1:20}$ is shown as a function of pore diameter D_v in Fig. 2. According to the BJH desorption method, the corresponding BET

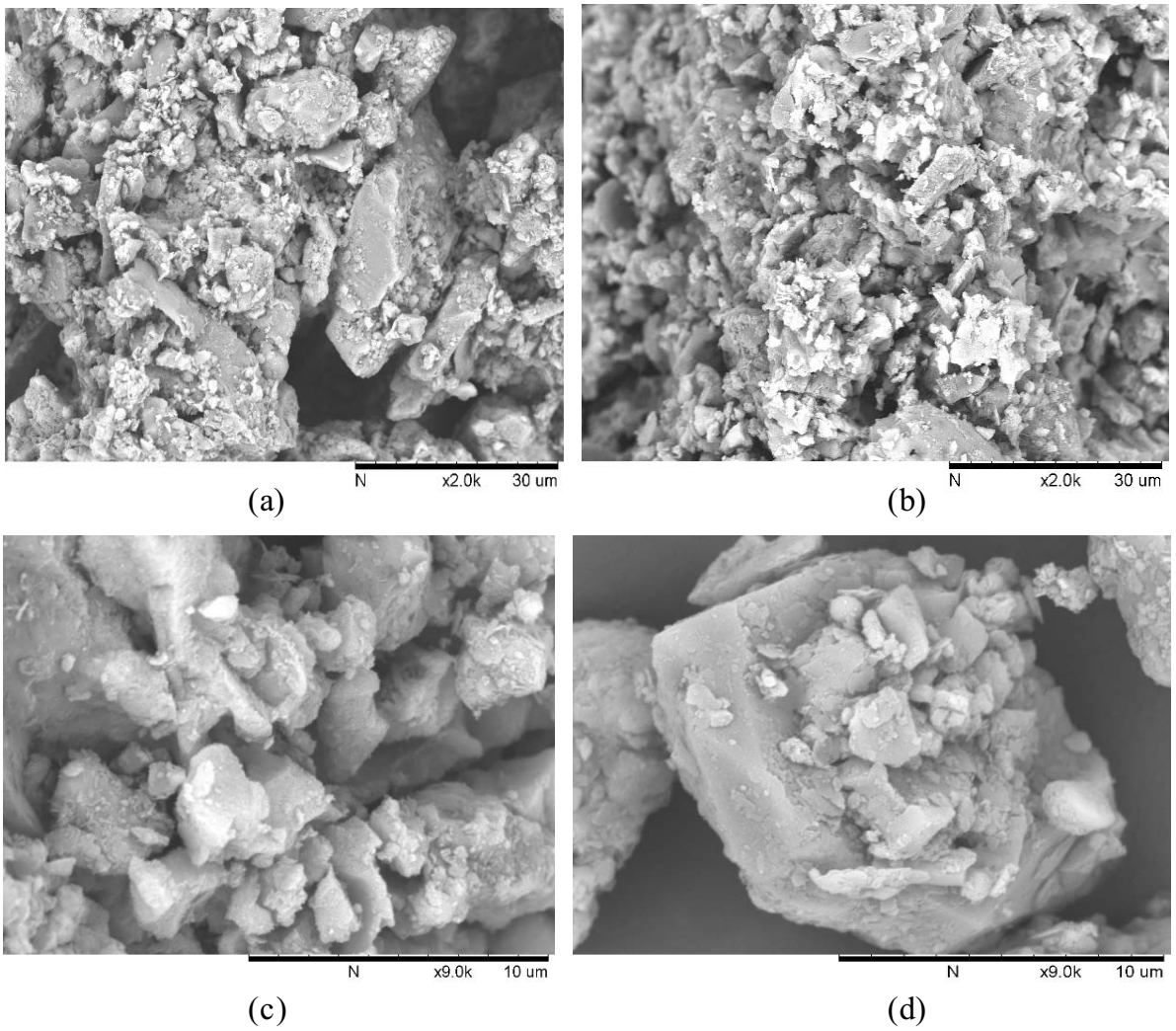

Fig. 1. SEM images of nanoparticles MNFFA with S/L = 1:20 at different magnifications: (a) original and (b) modified fly ash with a magnification of 2,000 times, and (c) original and (d) modified fly ash with a magnification of 9,000 times.

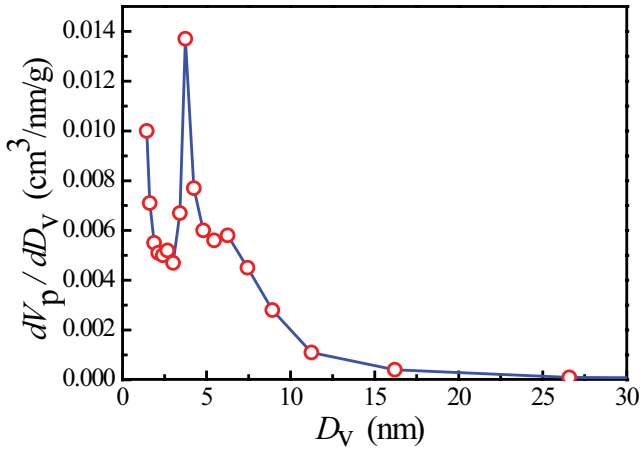

Fig. 2. The pore size distribution of the $MNFFA_{1:20}$.

specific surface area, pore diameter, and volume of the $MNFFA_{1:20}$ were determined to be 50.837 m^2/g, 3.738 nm, and 0.056 cm^3/g, respectively. In this case, the pore diameter obtained from the BJH model is usually slightly smaller than that from the density functional theory. This indicated that the synthesized sample contains numerous mesopores with pore diameters of approximately 3.7–4.0 nm.

The XRD images of the original fly ash and $MNFFA_{1:20}$ are presented in Figs. 3(a) and (b), respectively. Fig. 3(a) shows that Al_2O_3 (JCPDS No. 10-0425) and CaO (JCPDS No. 48-1467) associated with quartz (JCPDS No. 02-0471) are the main composition for the untreated coal fly ash. In Fig. 3(b), some peaks at 2θ = 35° (311), 43.2° (400), 51.7° (422), and

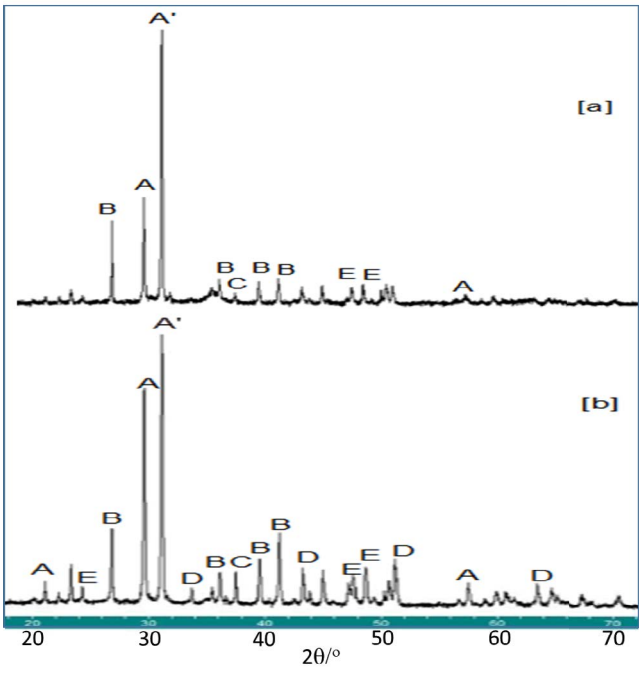

Fig. 3. XRD patterns of (a) original fly ash and (b) $MNFFA_{1:20}$ (A: SiO_2; A′: silicon aluminate; B: Al_2O_3; C: Fe_2O_3; D: Fe_3O_4; E: CaO).

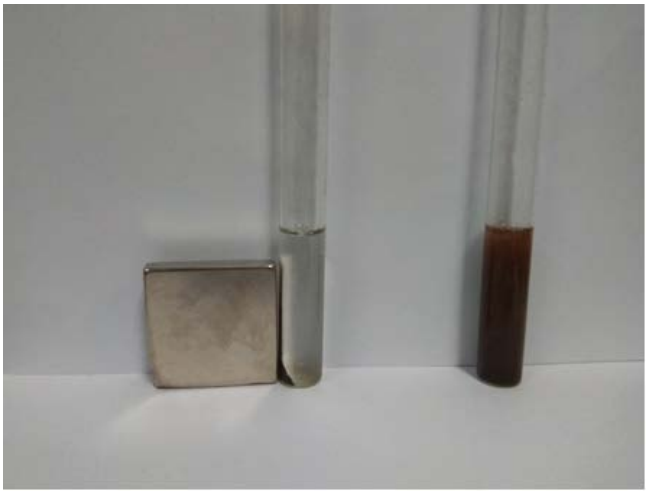

Fig. 4. Appearance of the aqueous solutions containing the adsorbent $MNFFA_{1:20}$ before (right) and after (left) an external magnetic field is applied.

63.8° (440) were appeared in the diffraction pattern of the MNFFA, which matched the standard cubic Fe_3O_4 (JCPDS No. 19-0629). This result is in conformity with the experimental results that the $MNFFA_{1:20}$ could be separated easily and quickly from the solution after absorption by applying a magnetic field. As demonstrated in Fig. 4, the original solution, which contains the $MNFFA_{1:20}$, is muddy after adsorption, while its appearance becomes transparent by applying an external magnetic field.

3.2. Adsorption capacity of different adsorbents

Table 1 shows the adsorption capacity of Cu^{2+} on the adsorbents with different compositions. Here the mass of the adsorbents used is W = 100 mg and the volume of the solutions is V = 100 mL. At the same initial concentration of Cu^{2+} (100 mg/L), the $MNFFA_{1:20}$ has a maximum adsorption capacity. The MNFFA can be separated easily and quickly from the solutions by applying a magnetic field within 30 s. Therefore the $MNFFA_{1:20}$ was chosen as an adsorbent in our subsequent tests.

3.3. Effect of equilibration time

The adsorption experiments were carried out with the time varied from 0 to 12 h using 200 mg $MNFFA_{1:20}$ and 100 mL aqueous solutions with 100 mg/L of Cr^{3+}, Cu^{2+}, or Ni^{2+} at 298 K and pH = 4.0. The adsorption efficiency of Cr^{3+}, Cu^{2+}, and Ni^{2+} as a function of equilibration time is presented in Fig. 5. It is clear that the adsorption efficiency of Cr^{3+}, Cu^{2+}, and Ni^{2+} is highly time-dependent. The longer adsorption time, the higher adsorption efficiency before the adsorption equilibrium is reached. The equilibrium was reached within 4 h for Cr^{3+} and Cu^{2+} ions, but 12 h is required for equilibration of adsorption of Ni^{2+}. The removal rate of heavy metal ions and adsorption efficiency are in the order: $Cu^{2+} > Cr^{3+} > Ni^{2+}$. The equilibrium adsorption capacity for Cr^{3+}, Cu^{2+}, and Ni^{2+} are 50.0, 50.0, and 19.2 mg/g, respectively.

Table 1
Adsorption quantities of Cu^{2+} on the adsorbents with different compositions

Adsorbents	Initial concentration (mg/L)	Equilibrium concentration (mg/L)	Adsorption quantity (mg/g)
MNFFA (*S*/*L* = 1/5)	100	2.19	97.81
MNFFA (*S*/*L* = 1/10)	100	1.13	98.87
MNFFA (*S*/*L* = 1/15)	100	1.27	98.73
MNFFA (*S*/*L* = 1/20)	100	0.63	99.37
MNFFA (*S*/*L* = 1/25	100	1.16	98.84
Pure Fe_3O_4	100	67.48	32.52
Pure fly ash	100	22.43	77.57

3.4. Effect of pH

As can be deduced from the surface characteristics and composition of the MNFFAs, the adsorbent used in this work has a porous structure with hydrophilic surfaces. The interaction between metal ions and adsorbent surfaces highly depends on pH of solutions. The pH of the aqueous solution is an important controlling parameter in heavy metal ions adsorption processes. In order to explore the effect of pH, we prepared a series of 100 mL Cr^{3+}, Cu^{2+}, and Ni^{2+} aqueous solutions with the initial concentration of 100 mg/L and pH = 3, 4, 7, and 9. And then 200 mg $MNFFA_{1:20}$ was introduced to the each solution for adsorption at 298 K.

The obtained adsorption efficiencies of Cr^{3+}, Cu^{2+}, and Ni^{2+} ions from aqueous solutions by the $MNFFA_{1:20}$ at equilibration time of 24 h and different pH values are plotted in Fig. 6. As the pH in solution is increased, the adsorption efficiency increases for all the studied cations. Fig. 6 illustrates that the adsorption efficiency for Ni^{2+} gradually increases from 21.8% to 49.68% when the pH varies from 3.0 to 9.0. Further increase of pH influences the adsorption efficiencies of Cr^{3+} and Cu^{2+} due to that adsorption of these two metal ions can reach equilibrium quickly (12 h) at pH = 3.0. It should be pointed out that the determination of reliable adsorption capacity is impossible at a higher pH due to the precipitation of cations by hydroxides.

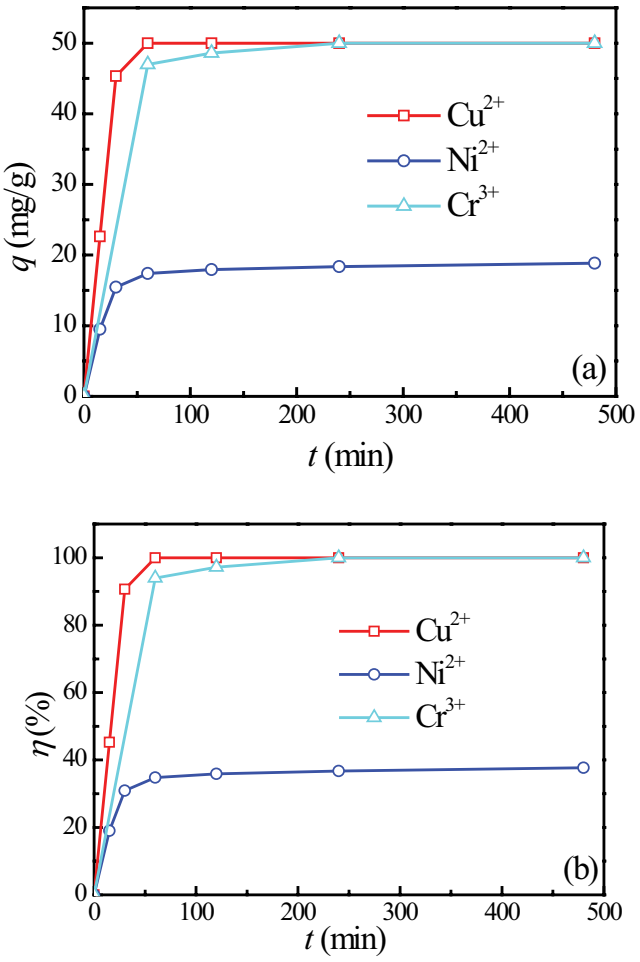

Fig. 5. Adsorption (a) quantity and (b) efficiency of three heavy metal ions on the $MNFFA_{1:20}$ in aqueous solution with metal ion concentration of 100 mg/L at *W*/*V* = 2.0 g/L, 298 K, and pH = 4.0.

3.5. Effect of dosage of $MNFFA_{1:20}$

Different dosages of the $MNFFA_{1:20}$ also influence the adsorption kinetics and equilibrium concentrations. The effect of dosage of the $MNFFA_{1:20}$ on adsorption efficiency and the adsorption capacity can be observed by adding different dosages of the $MNFFA_{1:20}$ to 100 mg/L initial solutions. The equilibrium adsorption capacities at different values of *W*/*V* are plotted in Fig. 7.

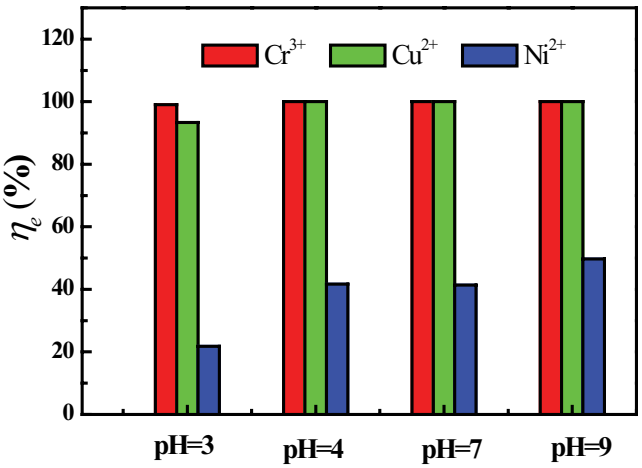

Fig. 6. Effect of pH on removal efficiency of heavy metal ions by the $MNFFA_{1:20}$ at C_0 = 100 mg/L, *W*/*V* = 2.0 g/L and 298 K.

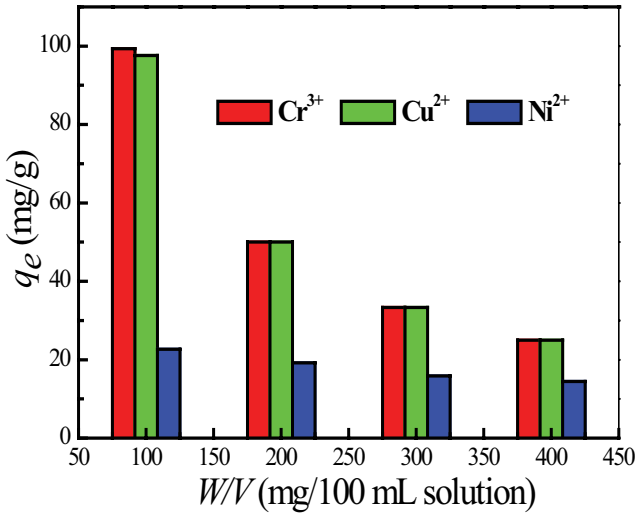

Fig. 7. Effect of adsorbent dosage on equilibrium adsorption quantity on the $MNFFA_{1:20}$ at C_0 = 100 mg/L, pH = 4.0 and 298 K.

With the increase of the dosage of the $MNFFA_{1:20}$, the adsorption rate is improved, but the equilibrium adsorption quantity per gram is reduced in Fig. 7. For both Cu^{2+} and Cr^{3+}, the maximum adsorption quantity per gram of the $MNFFA_{1:20}$ was 100 mg/g when 100 mg $MNFFA_{1:20}$ was introduced to 100 mL aqueous solution containing a heavy metal ion. But it needs a longer time to get maximum adsorption efficiency. Taking into account the effects of both adsorption rate and equilibrium capacity, the most suitable dosage of the $MNFFA_{1:20}$ is W/V = 2.0 g/L for Cu^{2+} and Cr^{3+}. For Ni^{2+} the highest adsorption quantity was obtained to be 19.21 mg/g, at W/V = 3.0 g/L, which is the best proportion of the $MNFFA_{1:20}$ in aqueous Ni^{2+} solution.

3.6. Effect of temperature

For all the investigated ions, experiments were conducted by varying the temperature between 298 and 313 K at C_0 = 100 mg/L, W/V = 2.0 g/L and pH = 4.0. Fig. 8 shows the removal efficiency evolution during the adsorption equilibration for Cr^{3+}, Cu^{2+}, and Ni^{2+} at different temperatures. As can be observed for the three ions, the highest adsorption capacity could be reached much faster at a higher temperature than that at a lower temperature. The higher the temperature, the shorter the equilibration time. The temperature above 303 K has a marginal effect on adsorption kinetics as can be observed in Fig. 8.

3.7. Adsorption kinetics

In order to better analyze the adsorption rates of Cr^{3+}, Cu^{2+}, and Ni^{2+} on the $MNFFA_{1:20}$, three simple kinetic models were tested. The pseudo-first-order rate expression, popularly known as the Lagergren equation [36,37], is generally described by the following equation:

$$\frac{dq}{dt} = k_1\left(q_e - q\right) \tag{3}$$

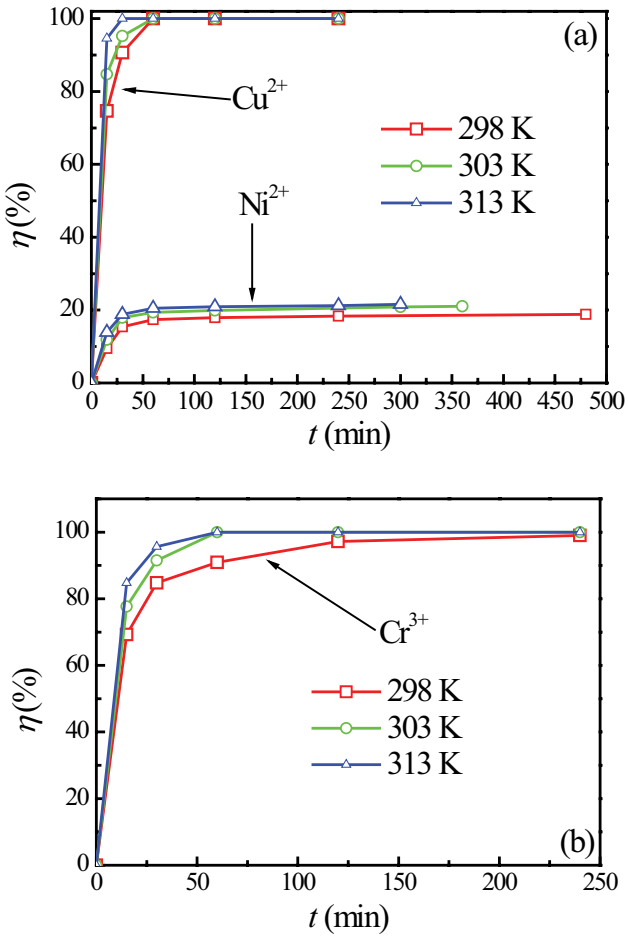

Fig. 8. The removal efficiency evolution during the equilibration of adsorption in single cationic solutions at C_0 = 100 mg/L, W/V = 2.0 g/L, pH = 4.0 and 298, 303, and 313 K: (a) Cu^{2+} and Ni^{2+} and (b) Cr^{3+}.

where q_e and q are the amount of the metal ions adsorbed per unit weight of sorbent (mg/g) at equilibrium and any equilibration time t, respectively. k_1 is the rate constant (h^{-1}). Integrating with appropriate boundary conditions (q = 0 for t = 0), we have

$$\ln\left(q_e - q\right) = \ln q_e - k_1 t \tag{4}$$

The adsorption data were also analyzed in terms of pseudo-second-order model given by the following equation:

$$\frac{dq}{dt} = k_2\left(q_e - q\right)^2 \tag{5}$$

where k_2 is the rate constant (mg g^{-1} h^{-1}). The linearized form of the pseudo-second-order model is written as follows:

$$\frac{t}{q} = \frac{1}{\left(k_2 q_e\right)} + \frac{t}{q_e} \tag{6}$$

The intraparticle diffusion model is given by the following equation:

$$q = k_{id} t^{1/2} + C \tag{7}$$

where k_{id} is the intraparticle diffusion rate constant (mg/g/h), and C is the intercept (mg/g).

The fitting parameters for both pseudo-first-order and pseudo-second-order models as well as intraparticle diffusion model are listed in Table 2. Also included in the table are the linear correlation coefficients (R^2) of the experimental data for the three models. It should be pointed out that the parameters of the three kinetic models are regressed based on the experimental adsorption data at W/V = 1.0 g/L for Cu^{2+} and Cr^{3+} and W/V = 2.0 g/L for Ni^{2+}. For all the three metal ions, the adsorption quantities are more relevant to time in terms of the pseudo-second-order model than those in terms of the pseudo-first-order or intraparticle diffraction model. The pseudo-first-order model only fits well the adsorption dynamics of Cu^{2+}. It is not suitable for the fitting of adsorption dynamic data of Cr^{3+} and Ni^{2+} on the $MNFFA_{1:20}$. The correlation coefficients are approximately the same for all the three metal ions, with values of larger than 0.999. The high correlation coefficients (R^2) for the pseudo-second-order kinetic model indicate that the adsorption of Cu^{2+}, Cr^{3+}, and Ni^{2+} on the MNFFA follows a second-order mechanism, likely controlled by the chemisorption.

3.8. Adsorption isotherms

Experimental data obtained from the batch equilibrium tests can be analyzed using the sorption isotherm models of Langmuir and Freundlich [36–38]. Langmuir sorption isotherm is the best known of all isotherms describing sorption and it has been successfully applied to many sorption processes. It is given by the following equation:

$$\frac{C_e}{q_e} = \frac{1}{bq_m} + \frac{C_e}{q_m} \tag{8}$$

where C_e is the equilibrium aqueous metal ions concentration (mg/L), q_e is the amount of metal ions adsorbed per gram of adsorbent at equilibrium (mg/g), q_m and b are the Langmuir constants related to the maximum adsorption capacity and energy of adsorption, respectively. The values of q_m (mg/g) and b (L/mg) can be determined from a linear fit of C_e/q_e versus C_e.

Freundlich isotherm is frequently used to describe the adsorption of inorganic and organic components in solutions. This empirical isotherm, which is appropriate to a nonideal heterogeneous adsorption, is expressed by the following equation:

$$\log q_e = \log K_f + \frac{1}{n}\log C_e \tag{9}$$

where K_f is roughly an indicator of the adsorption capacity and $1/n$ stands for the adsorption intensity. The magnitude of $1/n$ gives an indication of the favorability of adsorption. Values of n (where $n > 1$) represent favorable adsorption condition. Values of K_f and n can be determined from the slope and intercept of the plot of $\log q_e$ versus $\log C_e$.

In the equilibrium adsorption experiments, the initial concentrations of Cr^{3+} or Cu^{2+} in the solutions are 100, 200, 300, 500, and 700 mg/L and those of Ni^{2+} are 25, 50, 100, 200, and 300 mg/L. The equilibrium concentrations were measured after the systems were equilibrated for 24 h. And then the equilibrium adsorption quantities were calculated. Parameters of Langmuir and Freundlich isotherms for Cr^{3+}, Cu^{2+}, and Ni^{2+} were determined according to the linear correlations expressed by Eqs. (8) and (9). Their values were listed in Table 3.

As can be seen from Table 3, the linear correlation of the Langmuir model is higher than that of the Freundlich model in all cases studied in this work. The values of R^2 in terms of the Langmuir model are from 0.9985 to 0.9993, and the data have good stability. It means the Langmuir model represents a better fit to the experimental data than the Freundlich model does (0.958–0.977), which demonstrates that monolayer coverage of the heavy metal ions is formed at the outer surface of the MNFFA. The adsorption capacity in mg/g for the studied ions is in the order $Cu^{2+} > Cr^{3+} > Ni^{2+}$. This sequence is in

Table 2
Kinetic parameters for adsorption of metal ions on the $MNFFA_{1:20}$ at 298 K and pH = 4.0

Ion	Pseudo-first-order			Pseudo-second-order			Intraparticle diffusion		
	q_e (mg/g)	k_1 (h^{-1})	R^2	q_e (mg/g)	k_2 (g/mg/h)	R^2	k_{id} (mg/g/h)	C (mg/g)	R^2
Cu^{2+}	90.02	1.2	0.995	100.0	0.034	0.9992	53.14	0.334	0.973
Cr^{3+}	46.53	0.6	0.851	100.0	0.030	0.9999	51.73	15.712	0.897
Ni^{2+}	6.68	0.3	0.605	20.0	0.300	0.9997	6.55	2.559	0.925

Table 3
Parameters of Langmuir and Freundlich models for adsorption of metal ions on the $MNFFA_{1:20}$ at 298 K and pH = 4.0

Metal ion	Langmuir model			Freundlich model		
	q_m (mg/g)	b (L/mg)	R^2	K_f(L/mg)	n	R^2
Cu^{2+}	229.88	0.649	0.9993	126.83	8.656	0.9772
Cr^{3+}	212.31	0.459	0.9989	115.29	8.768	0.9467
Ni^{2+}	26.18	0.154	0.9985	18.33	17.364	0.9581

consistence with the affinity order of the metal ions toward the fly ash [39], microwaved olive stone activated carbon [40], carbon nanotubes [41], sawdust and modified peanut husk [42], hydrocolloid liquid-core capsules [43], and graphene oxide membranes [44].

According to density functional theory of electric double layer [45–47], the adsorption capacity of a counterion adsorbed on the surface or in the pore of the adsorbent depends strongly on the ionic valence and size as well as the interaction force between the ion and the surface (external potential). A stronger attractive external potential and a higher ionic valence may result in a higher adsorption capacity while a larger ionic diameter may play an opposite role to adsorption. The interaction between metal ion and the surface of the adsorbent should be precipitation, adsorption, and/or ion-exchange. If the precipitation is assumed to be the main factor, the solubility product K_{sp} for $Cu(OH)_2$, $Cr(OH)_3$, and $Ni(OH)_2$ determines the external potential applied on Cu^{2+}, Cr^{3+}, and Ni^{2+}, respectively, due to the hydrophilic surface of the MNFFA. The values of pK_{sp} for $Cu(OH)_2$, $Cr(OH)_3$, and $Ni(OH)_2$ at 298.15 K are 19.36 [48], 28.36 [49], and 16.10 [50], respectively. Therefore the external potential of the adsorbent applied on the metal ions should be in the order $Cr^{3+} >> Cu^{2+} > Ni^{2+}$. Meanwhile, the effective cationic diameters can be estimated from the experimental activity coefficient data [51] in terms of the modified mean-spherical approximation [52,53] and their values are $\sigma_0(Cu^{2+})$ = 8.63 Å, $\sigma_0(Cr^{3+})$ = 9.74 Å, and $\sigma_0(Ni^{2+})$ = 9.28 Å. Based on the external potentials and ionic diameters of the metal ions, one can understand that the adsorption capacity of Cr^{3+} should be the highest due to the very strong external potential applied by the surface although the largest size of Cr^{3+} may cancel some capacity. The adsorption capacity of Cu^{2+} should be apparently greater than that of Ni^{2+} due to that Cu^{2+} has a stronger external potential and a smaller size. Overall, the electrolyte theory predicts the adsorption capacity in the order $Cr^{3+} > Cu^{2+} > Ni^{2+}$, which is in accordance with the experimental sequence in mmol/g. The experimental adsorption capacities of Cu^{2+}, Cr^{3+}, and Ni^{2+} are 3.62, 4.08, and 0.45 mmol/g, respectively. From above analysis based on the binding interactions and electrostatic effects from the DFT, we concluded that the enhancement of the adsorption is mainly due to Fe-OH, Si-OH, Al-OH, and Ca-OH groups on the surface of the MNFFA material by precipitation interactions and volume effect of the metal ions.

In Table 4, we compared the $MNFFA_{1:20}$ with recently reported adsorbents for the removal of the heavy metal ions studied in this work. Although it is hard to come to a complete conclusion from the simple comparison due to different solution conditions, the adsorption capacities of the $MNFFA_{1:20}$ are very competitive with other sorbents, especially for the removal of Cu^{2+} and Cr^{3+}.

3.9. Co-adsorption of mixed metal ions

We have also investigated the adsorption of heavy metal ions in mixed cationic solutions. The adsorption quantities of metal ions from the binary cationic solution varying with the adsorption equilibration time are demonstrated in Fig. 9. The selectivity of Cu^{2+} over Cr^{3+} and Ni^{2+}, Cr^{3+} over Ni^{2+} is, respectively, 1.06, 8.68, and 2.98 in corresponding binary cationic solutions at W/V = 2.0 g/L, pH = 4.0, and temperature T = 298 K. From these figures we can see that adsorption rate is slower in solutions containing two metal ions than that contain single metal ion. This is because the introduction of the second ion decreases the activity coefficient of both metal ions in the low ionic strength region. In addition, there exists an adsorption competition between the two metal ions. It is clearly shown in Figs. 9(a) and (b) that the introduction of Cr^{3+} or Ni^{2+} to aqueous Cu^{2+} solution has only marginal effect on both adsorption equilibrium and kinetics for Cu^{2+}, while Cu^{2+} substantially reduces both adsorption equilibria and kinetics of Cr^{3+} and Ni^{2+} in the binary cationic solutions. It means that in the binary cationic solutions, the $MNFFA_{1:20}$

Table 4
Comparison of the maximum adsorption capacities of present work with those of recent investigations

Metal ion	Adsorbent	q_m (mg/g)	Reference
Cu^{2+}	Peach palm sheath colonized with *Agaricus blazei*	22.14	[54]
	Microwaved olive stone activated carbon	22.73	[40]
	Graphene oxide membrane	72.60	[44]
	Poly(MVE-alt-MA-I)	81.72	[55]
	Hydrocolloid liquid-core capsules	219.00	[43]
	Magnetic nanoparticles of Fe_3O_4-base modified fly ash	229.88	This work
Cr^{3+}	Peach palm sheath colonized with *Agaricus blazei*	19.42	[54]
	Poly(MVE-alt-MA-I)	29.97	[55]
	Mn_3O_4 nanomaterial	41.7	[56]
	Magnetic nanoparticles of Fe_3O_4-base modified fly ash	212.31	This work
Ni^{2+}	Microwaved olive stone activated carbon	12.00	[40]
	Graphene oxide membrane	62.30	[44]
	Hydrocolloid liquid-core capsules	65.00	[43]
	Poly(MVE-alt-MA-I)	67.45	[55]
	Magnetic nanoparticles of Fe_3O_4-base modified fly ash	26.18	This work

has a preferential adsorption of Cu^{2+} than Cr^{3+} and Ni^{2+} when the bulk ionic concentrations are the same. These results can be well understood in terms of the effective ionic diameter and external potential of the adsorbent surface on each ion.

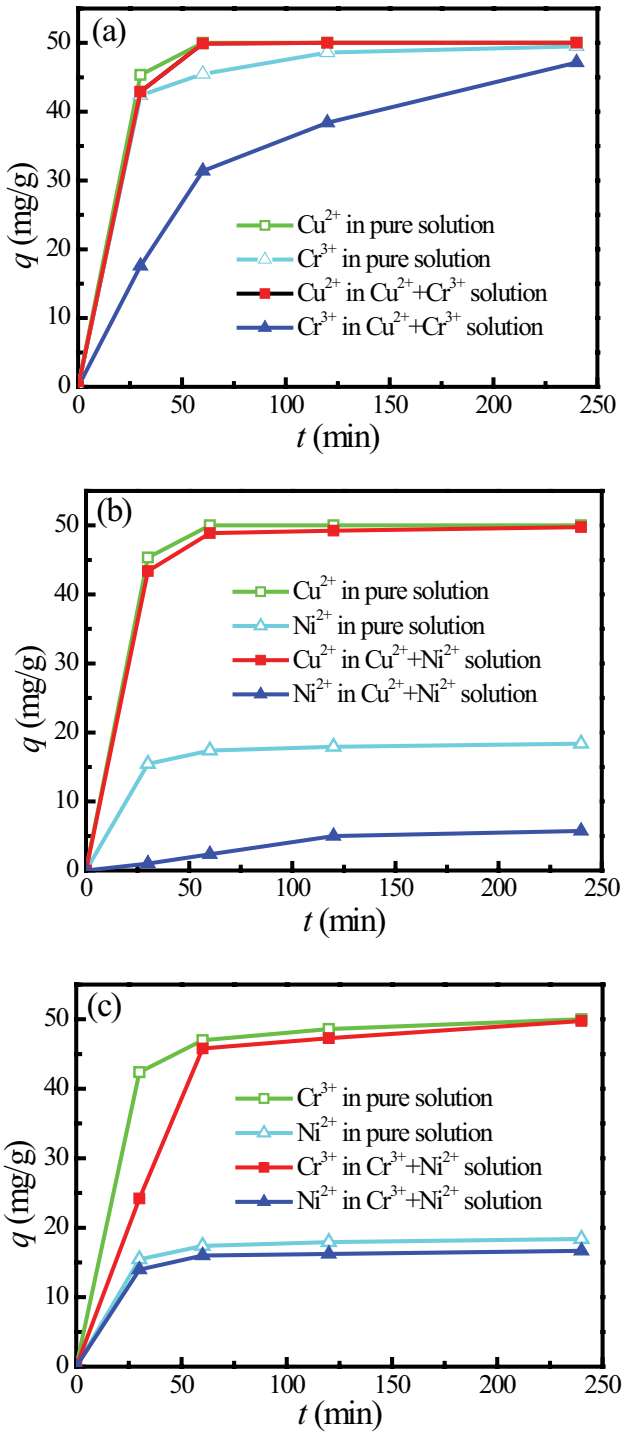

Fig. 9. Comparison of adsorption quantities in pure and binary cationic solutions: (a) $Cu^{2+} + Cr^{3+}$, (b) $Cu^{2+} + Ni^{2+}$, and (c) $Cr^{3+} + Ni^{2+}$ at W/V = 2.0 g/L, pH = 4.0 and temperature T = 298 K. The concentration for each ion in pure and binary cationic solutions is 100 mg/L.

The Cu^{2+} is adsorbed in the small pores where Ni^{2+} and Cr^{3+} cannot be adsorbed due to the smallest size and the moderate external potential of Cu^{2+}. The adsorption quantity and rate for Cr^{3+} decrease to a lesser extent compared with Ni^{2+} because the external potential acting on Cu^{2+} is weaker than that on Cr^{3+} and stronger than that on Ni^{2+}.

Fig. 9(c) demonstrates that both adsorption rate and quantity of Cr^{3+} and Ni^{2+} are decreased in a small extent due to the reduction of the ionic activity. There is no competitive adsorption between Cr^{3+} and Ni^{2+} because Cr^{3+} cannot enter the adsorption sites of Ni^{2+} due to the size effect and Ni^{2+} cannot occupy the adsorption sites of Cr^{3+} due to the extremely strong external potential on Cr^{3+}. Therefore, the $MNFFA_{1:20}$ almost has no selectivity between Cr^{3+} and Ni^{2+}.

The evolution of the adsorption quantity for Cu^{2+}, Cr^{3+}, and Ni^{2+} is plotted in Fig. 10 for the ternary cationic solutions at W/V = 2.0 g/L and the concentration of each metal ion is 100 mg/L. The selectivity of Cu^{2+} over Cr^{3+} and Ni^{2+} is, respectively, 1.21 and 4.67 in the ternary cationic solution at W/V = 2.0 g/L, pH = 4.0, and temperature T = 298 K. As expected, there is almost no effect on the adsorption equilibrium and kinetics of Cu^{2+} as can be seen from Fig. 10. The adsorption quantity and rate of Cr^{3+} are reduced to a moderate extent and those of Ni^{2+} are decreased substantially. Again these selective properties can be well explained by the ionic size and external potential obtained in the above section.

3.10. Desorption and regeneration of adsorbent

Adsorption of the heavy metal ions may leave a heavy burden on the environment and thus the exhausted $MNFFA_{1:20}$ should be regenerated for recycling. Based on the recovery efficiency of metal ions, NaOH was selected as eluent after trying other acids. The desorption of metal ions from the absorbent was achieved by putting 0.01 M NaOH solution into the column for 24 h in oscillator. Fig. 11 illustrates the adsorption and desorption behavior of the

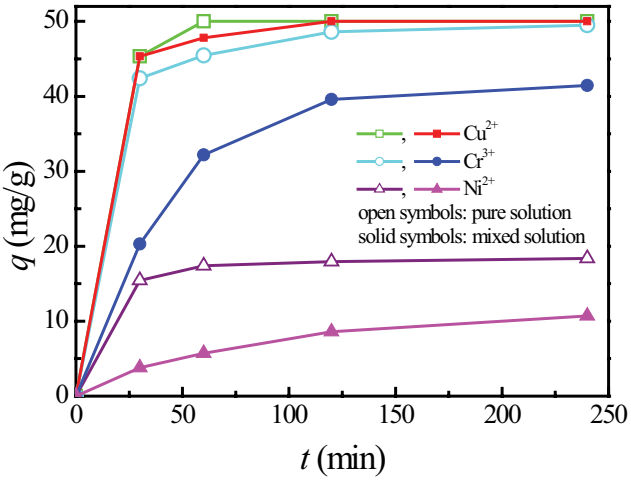

Fig. 10. Comparison of adsorption quantities in pure and ternary cationic ($Cu^{2+} + Cr^{3+} + Ni^{2+}$) solution at W/V = 2.0 g/L, pH = 4.0, and temperature T = 298 K. The concentration for each ion in pure and ternary cationic solutions is 100 mg/L.

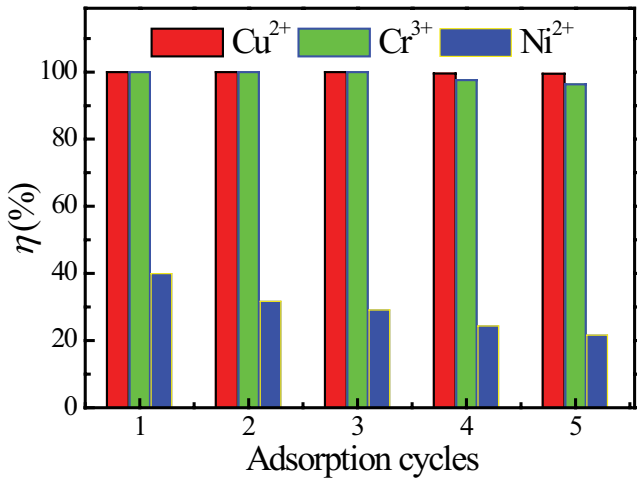

Fig. 11. The removal efficiency as a function of adsorption cycles.

$MNFFA_{1:20}$ porous monoliths. After five cycles, the adsorption efficiency of Cu^{2+}, Cr^{3+}, and Ni^{2+} gradually decreased from 100% to 99.5%, from 100% to 96.34%, and from 39.95% to 21.64%, respectively. These experimental results infer that the $MNFFA_{1:20}$ has stable physical and chemical properties and adsorption capacity for reuse.

4. Conclusion

In this work, magnetic nanoparticles composed of Fe_3O_4 and alkali-treated coal fly ash were synthesized in order to treat the water polluted by heavy metal ions such as Cr^{3+}, Cu^{2+}, and Ni^{2+}. The synthesized magnetic Fe_3O_4@alkali-treated coal fly ash was characterized using the SEM, XRD, and BET method. Experimental results indicate the maximum theoretical adsorption capacity in the investigated conditions was 229.88, 212.31, and 26.18 mg/g for Cu^{2+}, Cr^{3+}, and Ni^{2+}, respectively. The adsorption mechanism is proposed to be a pore accommodation and binding between metal ions and nanoparticles influenced by the effective ionic diameters and external potential exerted on the metal cations. Analyses of experimental data indicated that the adsorption equilibrium and kinetics of all the investigated ions onto the $MNFFA_{1:20}$ follow the Langmuir and pseudo-second-order models, respectively. The prepared adsorbent exhibits high Cu^{2+} selectivity in all binary and ternary mixed ionic solutions of Cu^{2+}, Cr^{3+}, and Ni^{2+}. The selectivity of Cu^{2+} over Cr^{3+} and Ni^{2+} is, respectively, 1.21 and 4.67 in the ternary cationic solutions. The adsorption efficiency of Cu^{2+}, Cr^{3+}, and Ni^{2+} can be kept for five adsorption cycles. Besides, a quick separation can be carried out without secondary pollution by using the $MNFFA_{1:20}$. Therefore, we concluded that the $MNFFA_{1:20}$ with a fine grain size (3.738 nm) is an effective, convenient, low-cost, and environment-friendly material for the removal and recovery of heavy metals from the polluted water.

Acknowledgments

The authors are grateful to Yong-Jun Du and Yi-Bai He for their help during the research work and the preparation of the manuscript. Some discussions on the research given by Prof. Jianguo Mi are also highly appreciated. This research is supported by the National Natural Science Foundation of China under grant no. 21676154.

References

[1] V.K. Gupta, O. Moradi, I. Tyagi, S. Agarwal, H. Sadegh, R. Shahryari-Ghoshekandi, A.S.H. Makhlouf, M. Goodarzi, A. Garshasbi, Study on the removal of heavy metal ions from industry waste by carbon nanotubes: effect of the surface modification: a review, Crit. Rev. Environ. Sci. Technol., 46 (2016) 93–118.
[2] B. He, Z.J. Yun, J.B. Shi, Research progress of heavy metal pollution in China: sources, analytical methods, status and toxicity, Chin. Sci. Bull., 58 (2013) 134–140.
[3] H. Javadian, Adsorption performance of suitable nanostructured novel composite adsorbent of poly(N-methylaniline) for removal of heavy metal from aqueous solutions, J. Ind. Eng. Chem., 20 (2014) 4344–4352.
[4] R.W. Peters, Chelant extraction of heavy metals from contaminated soils, J. Hazard. Mater., 66 (1999) 151–210.
[5] K. Olie, P.L. Vermeulen, O. Hutzinger, Chlorodibenzo-p-dioxins and chlorodib-enzofurans are trace components of fly ash and flue gas of some municipal incinerators in the Netherlands, Chemosphere, 61 (1977) 455–459.
[6] F.L. Fu, Q. Wang, Removal of heavy metal ions from wastewaters: a review, J. Environ. Manage., 92 (2011) 407–418.
[7] M. Naushad, S. Vasudevan, G. Sharma, A. Kumar, Z.A. ALOthman, Adsorption kinetics, isotherms and thermodynamic studies for Hg^{2+} adsorption from aqueous medium using alizarin red-S-loaded amberlite IR4-400 resin, Desal. Wat. Treat., 57 (2016) 18551–18559.
[8] K. Chithra, K. Dhivya, Modification and characterization of solid waste: an effective adsorbent for heavy metal removal, Desal. Wat. Treat., 67 (2017) 168–177.
[9] J. Ayala, F. Blanco, P. Garcia, P. Rodriguez, J. Sancho, Asturian fly ash as a heavy metals removal material, Fuel, 77 (1998) 1147–1154.
[10] S.S. Banerjee, R.V. Jayaram, M.V. Joshi, Removal of nickel (II) and zinc (II) from wastewater using fly ash and impregnated fly ash, Sep. Sci. Technol., 38 (2003) 1015–1032.
[11] H.A. Asmaly, Ihsanullah, B. Abussaud, T.A. Saleh, T. Laoui, V.K. Gupta, M.A. Atieh, Adsorption of phenol on aluminum oxide impregnated fly ash, Desal. Wat. Treat., 57 (2016) 6801–6808.
[12] C.J. An, S.Q. Yang, G.H. Huang, S. Zhao, P. Zhang, Y. Yao, Removal of sulfonated humic acid from aqueous phase by modified coal fly ash waste: equilibrium and kinetic adsorption studies, Fuel, 165 (2016) 264–271.
[13] S.A. Bernal, J.L. Provis, B. Walkley, R.S. Nicolas, J.D. Gehman, D.G. Brice, A.R. Kilcullen, P. Duxson, J.S.J. van Deventer, Gel nanostructure in alkali-activated binders based on slag and fly ash, and effects of accelerated carbonation, Cement Concrete Res., 53 (2013) 127–144.
[14] K.S. Hui, C.Y.H. Chao, S.C. Kot, Removal of mixed heavy metal ions in wastewater by zeolite 4A and residual products from recycled coal fly ash, J. Hazard. Mater., 127 (2005) 89–101.
[15] B.P. Kelleher, M.N. O'Callaghan, M.J. Leahy, T.F. O'Dwyer, J.J. Leahy, The use of fly ash from the combustion of poultry litter for the adsorption of chromium (III) from aqueous solution, J. Chem. Technol. Biotechnol., 77 (2002) 1212–1218.
[16] M. Visa, A.M. Chelaru, Hydrothermally modified fly ash for heavy metals and dyes removal in advanced wastewater treatment, Appl. Surf. Sci., 303 (2014) 14–22.
[17] Z.A. AL-Othman, R. Ali, M. Naushad, Hexavalent chromium removal from aqueous medium by activated carbon prepared from peanut shell: adsorption kinetics, equilibrium and thermodynamics studies, Chem. Eng. J., 184 (2012) 238–247.
[18] Z.A. AL-Othman, M. Naushad, R. Ali, Kinetics, equilibrium isotherm and thermodynamic studies of Cr(VI) adsorption onto low-cost adsorbent developed from peanut shell activated with phosphoric acid, Environ. Sci. Pollut. Res., 20 (2013) 3351–3365.

[19] M. Naushad, Z.A. ALOthman, M.M. Alam, M.R. Awual, G.E. Eldesoky, M. Islam, Synthesis of sodium dodecyl sulfate-supported nanocomposite cation exchanger: removal and recovery of Cu^{2+} from synthetic, pharmaceutical and alloy samples, J. Iran. Chem. Soc., 12 (2015) 1677–1686.
[20] M. Naushad, Z.A. ALOthman, M.R. Awual, M.M. Alam, G.E. Eldesoky, Adsorption kinetics, isotherms, and thermodynamic studies for the adsorption of Pb^{2+} and Hg^{2+} metal ions from aqueous medium using Ti(IV) iodovanadate cation exchanger, Ionics, 21 (2015) 2237–2245.
[21] J. Pizarro, X. Castillo, S. Jara, C. Ortiz, P. Navarro, H. Cid, H. Rioseco, D. Barros, N. Belzile, Adsorption of Cu^{2+} on coal fly ash modified with functionalized mesoporous silica, Fuel, 156 (2015) 96–102.
[22] A.M. Cardoso, A. Paprocki, L.S. Ferret, C.M.N. Azevedo, M. Pires, Synthesis of zeolite Na-P1 under mild conditions using Brazilian coal fly ash and its application in wastewater treatment, Fuel, 139 (2015) 59–67.
[23] J. Hizal, E. Tutem, K. Guclu, M. Hugul, S. Ayhan, R. Apak, F. Kilinckale, Heavy metal removal from water by red mud and coal fly ash: an integrated adsorption-solidification/stabilization process, Desal. Wat. Treat., 51 (2013) 37–39.
[24] M. Izquierdo, X. Querol, Leaching behavior of elements from coal combustion fly ash: an overview, Int. J. Coal Geol., 94 (2012) 54–66.
[25] H.C. Tao, T. Lei, G. Shi, X.N. Sun, X.Y. Wei, L.J. Zhang, W.M. Wu, Removal of heavy metals from fly ash leachate using combined bioelectrochemical systems and electrolysis, J. Hazard. Mater., 264 (2014) 1–7.
[26] B. Nowwak, P. Aschenbrenner, F. Winter, Heavy metal removal from sewage sludge ash and municipal solid waste fly ash – a comparison, Fuel Process. Technol., 105 (2013) 195–201.
[27] L. Giraldo, A. Erto, J.C. Moreno-Pirajan, Magnetite nanoparticles for removal of heavy metals from aqueous solutions: synthesis and characterization, Adsorption, 19 (2013) 465–474.
[28] A.A. Alqadami, M. Naushad, M.A. Abdalla, T. Ahamad, Z.A. ALOthman, S.M. Alshehri, Synthesis and characterization of Fe_3O_4@TSC nanocomposite: highly efficient removal of toxic metal ions from aqueous medium, RSC Adv., 6 (2016) 22679–22689.
[29] A.A. Alqadami, M. Naushad, M.A. Abdalla, M.R. Khan, Z.A. ALOthman, Adsorptive removal of toxic dye using Fe_3O_4-TSC nanocomposite: equilibrium, kinetic, and thermodynamic studies, J. Chem. Eng. Data, 61 (2016) 3806–3813.
[30] A.A. Alqadami, M. Naushad, M.A. Abdalla, T. Ahamad, Z.A. ALOthman, S.M. Alshehri, A.A. Ghfar, Efficient removal of toxic metal ions from wastewater using a recyclable nanocomposite: a study of adsorption parameters and interaction mechanism, J. Cleaner Prod., 156 (2017) 426–436.
[31] M. Naushad, T. Ahamad, B.M. Al-Maswari, A.A. Alqadami, S.M. Alshehri, Nickel ferrite bearing nitrogen-doped mesoporous carbon as efficient adsorbent for the removal of highly toxic metal ion from aqueous medium, Chem. Eng. J., 330 (2017) 1351–1360.
[32] A.A. Alqadami, M. Naushad, Z.A. ALOthman, A.A. Ghfar, Novel metal-organic framework (MOF) based composite materials for the sequestration of U(VI) and Th(IV) metal ions from aqueous environment, ACS Appl. Mater. Interfaces, 9 (2017) 36026–36037.
[33] A. Kumar, A. Kumar, G. Sharma, M. Naushad, F.J. Stadler, A.A. Ghfar, P. Dhiman, R.V. Saini, Sustainable nano-hybrids of magnetic biochar supported g-C_3N_4/$FeVO_4$ for solar powered degradation of noxious pollutants-Synergism of adsorption, photocatalysis & photo-ozonation, J. Cleaner Prod., 165 (2017) 431–451.
[34] A. Kumar, A. Kumar, G. Sharma, A.H. Al-Muhtaseb, M. Naushad, A.A. Ghfar, F.J. Stadler, Quaternary magnetic BiOCl/g-C_3N_4/Cu_2O/Fe_3O_4 nano-junction for visible light and solar powered degradation of the sulfamethoxazole from aqueous environment, Chem. Eng. J., 334 (2018) 462–478.
[35] Z.S. Chen, J. Wang, Z.X. Pu, Y.S. Zhao, D.H. Jia, H.X. Chen, T. Wen, B.W. Hu, A. Alsaedi, T. Hayat, X.K. Wang, Synthesis of magnetic Fe_3O_4/CFA composites for the efficient removal of U(VI) from wastewater, Chem. Eng. J., 320 (2017) 448–457.
[36] R.S. Blissett, N.A. Rowson, A review of the multi-component utilisation of coal fly ash, Fuel, 97 (2012) 1–23.
[37] S.O. Bada, J.H. Potgieter, A.S. Afolabi, Kinetics studies of adsorption and desorption of South African fly ash for some phenolic compounds, Part. Sci. Technol., 31 (2013) 1–9.
[38] S.P. Mishra, Adsorption-desorption of heavy metal ions, Curr. Sci., 107 (2014) 601–612.
[39] E. Pehlivan, S. Cetin, Application of fly ash and activated carbon in the removal of Cu^{2+} and Ni^{2+} ions from aqueous solutions, Energy Sources Part A, 30 (2008) 1153–1165.
[40] T.M. Alslaibi, I. Abustan, M.A. Ahmad, A.A. Foul, Application of response surface methodology (RSM) for optimization of Cu^{2+}, Cd^{2+}, Ni^{2+}, Pb^{2+}, Fe^{2+}, and Zn^{2+} removal from aqueous solution using microwaved olive stone activated carbon, J. Chem. Technol. Biotechnol., 88 (2013) 2141–2151.
[41] M. Tuzen, K.O. Saygi, M. soylak, Solid phase extraction of heavy metal ions in environmental samples on multiwalled carbon nanotubes, J. Hazard. Mater., 152 (2008) 632–639.
[42] Q. Li, J. Zhai, W. Zhang, M. Wang, J. Zhou, Kinetic studies of adsorption of Pb(II), Cr(III),and Cu(III) from aqueous solution by sawdust and modified peanut husk, J. Hazard. Mater., 141 (2007) 163–167.
[43] A. Nusssinovitch, O. Dagan, Hydrocolloid liquid-core capsules for the removal of heavy-metal cations from water, J. Hazard. Mater., 299 (2015) 122–131.
[44] P. Tan, J. Sun, Y.Y. Hu, Z. Fang, Q. Bi, Y.C. Chen, J.H. Cheng, Adsorption of Cu^{2+}, Cd^{2+} and Ni^{2+} from aqueous single metal solutions on graphene oxide membranes, J. Hazard. Mater., 297 (2015) 251–260.
[45] K. Wang, Y.-X. Yu, G.-H. Gao, Density functional study on the structural and thermodynamic properties of aqueous DNA-electrolyte solution in the framework of cell model, J. Chem. Phys., 128 (2008) 185101.
[46] B. Peng, Y.-X. Yu, Ion distributions, exclusion coefficients, and separation factors of electrolytes in a charged cylindrical nanopore: a partially perturbative density functional theory study, J. Chem. Phys., 131 (2009) 134703.
[47] Y. Xin, Y.-X. Zheng, Y.-X. Yu, Density functional theory study on ion adsorption and electroosmotic flow in a membrane with charged cylindrical pores, Mol. Phys., 114 (2016) 2328–2336.
[48] L. Hidmi, M. Edwards, Role of temperature and pH in $Cu(OH)_2$ solubility, Environ. Sci. Technol., 33 (1999) 2607–2610.
[49] J.W. Boclair, P.S. Braterman, J.P. Jiang, S.W. Lou, F. Yarberry, Layered double hydroxide stability. 2. Formation of Cr(III)-containing layered double hydroxides directly from solution, Chem. Mater., 11 (1999) 303–307.
[50] S.V. Mattigod, D. Rai, A.R. Felmy, L.F. Rao, Solubility and solubility product of crystalline $Ni(OH)_2$, J. Solution Chem., 26 (1997) 391–403.
[51] R.A. Robinson, R.H. Stokes, Tables of osmotic and activity coefficients of electrolytes in aqueous solution at 25°C, Trans. Faraday Soc., 45 (1949) 612–624.
[52] J.-F. Lu, Y.-X. Yu, Y.-G. Li, Modification and application of the mean spherical approximation method, Fluid Phase Equilibria, 85 (1993) 81–100.
[53] Y.-X. Yu, G.-H. Gao, Y.-G. Li, surface tension for aqueous electrolyte solutions by the modified mean spherical approximation, Fluid Phase Equilibria, 173 (2000) 23–38.
[54] C.L. Massocatto, M. de Andrade, A.C. Honorato, J. Caetano, C.R.T. Tarley, A.G. Junior, N.B. Colauto, G.A.L. Colauto, D.C. Dragunski, Biosorption of Pb^{2+}, Cr^{3+}, and Cu^{2+} by peach palm sheath modified colonized by *Agaricus blazei*, Desal. Wat. Treat., 57 (2016) 19927–19938.
[55] M. Ceglowski, G. Schroeder, Preparation of porous resin with Schiff base chelating groups for removal of heavy metal ions from aqueous solutions, Chem. Eng. J., 263 (2015) 402–411.
[56] Y. Cantu, A. Remes, A. Reyna, D. Martinez, J. Villarreal, H. Ramos, S. Trevino, C. Tamez, A. Martinez, T. Eubanks, J.G. Parsons, Thermodynamics, kinetics, and activation energy studies of the sorption of chromium (III) and chromium (VI) to a Mn_3O_4 nanomaterial, Chem. Eng. J., 254 (2014) 374–383.